Validating Prior-informed Fisher-matrix Analyses against GWTC Data

Ulyana Dupletsa ®,[1, 2, *] Jan Harms ®,[1, 2] Ken K. Y. Ng ®,[3] Jacopo
Tissino ®,[1, 2] Filippo Santoliquido ®,[1, 2] and Andrea Cozzumbo ®[1, 2]

[1] *Gran Sasso Science Institute (GSSI), I-67100 L'Aquila, Italy*
[2] *INFN, Laboratori Nazionali del Gran Sasso, I-67100 Assergi, Italy*
[3] *William H. Miller III Department of Physics and Astronomy,*
Johns Hopkins University, Baltimore, Maryland 21218, USA

Next-generation gravitational-wave detectors, such as the Einstein Telescope (ET), are expected to observe a few 100,000 signals each year. This will require efficient analysis tools and computational resources well beyond the needs of current detectors. Such resources are not presently available to the science community. Therefore, to investigate ET observational capabilities and science cases, Fisher-matrix methods are used to predict how precisely parameters like mass, spin, source distance or sky location can be estimated from ET data. The approach is based on a Gaussian approximation of the likelihood function. However, the reliability of error estimates obtained from Fisher-matrix methods remains an open question. In this article, we present a Fisher-matrix analysis of signals of the Gravitational Wave Transient Catalog (GWTC). We compare parameter-estimation errors obtained using the Fisher matrix code `GWFish` with the errors from the marginal distributions of the Virgo/LIGO posterior analysis. In order to understand the impact of prior distributions on the results, we implemented a Gaussian likelihood sampling algorithm with priors in `GWFish`. To ensure a fair comparison of the methods, the `GWFish` analyses presented in this article use the same priors and the same instrument-noise spectra as the Virgo/LIGO posterior analyses. Our findings imply that Fisher-matrix methods, especially if augmented with the use of priors, are a valid tool for ET science-case studies.

I. INTRODUCTION

The discovery of gravitational waves (GWs) marked a milestone in the scientific community. Since the first detected event in 2015 [1], we have successfully carried out three observational runs [2–4], the first half of the fourth observing run, and we are currently taking data for the second half of the fourth observing run. The statistics we are collecting are ever-growing. Furthermore, as the plans for the next-generation GW observatories, such as the Einstein Telescope (ET) [5–7] and the Cosmic Explorer (CE) [8, 9], are evolving, the need for advanced tools to interpret the wealth of data these instruments will provide us has never been more critical.

While the standard data analysis in the LIGO-Virgo-KAGRA (LVK) Collaboration relies on Bayesian parameter estimation [10–12], the science-case studies of future GW detectors pose a computational challenge that is currently addressed by Fisher-matrix techniques [13]. Fisher-matrix analysis [14] has become a customary approach to simulate the precision of parameter estimation for next-generation detectors, giving an analytic model for describing the GW signals. In recent years, various Fisher-matrix codes have been developed, in particular `GWBench` [15], `GWFish` [16], `GWFast` [17, 18], and `TiDoFM` [19, 20]. The main differences between the codes lie in the methods used for differentiation and matrix inversion, which are crucial steps in the analysis. However, the codes have undergone several successful cross-checks and output comparable results [13].

Even though Fisher matrix analysis is an approximate analysis technique based on Gaussian likelihood approximation expected to hold just for high signal-to-noise (SNR) signals [14], its strengths lie in being computationally fast (seconds of computational time against days for one event) and thus effective in large-scale simulations.

The standard Fisher analysis assumes the priors on the parameters to be uniform. In the high SNR limit, the likelihood is expected to be a narrowly peaked function around the maximum. Therefore, no prior information is needed. In practice, this is not the case. As we will see throughout the paper, correlations among parameters rather than low SNR can limit the accuracy of parameter errors under the Gaussian likelihood approximation without priors. It is crucial to include prior information to obtain more accurate posterior samples that do not overestimate errors by orders of magnitude and go beyond the physical range of parameters [21]. This issue has already been partially addressed in [17], and some applications are already present in [13].

The scope of the following paper is twofold. Firstly, we describe a computationally efficient method to incorporate priors into our Fisher-matrix code, `GWFish` [16]. The new feature allows us to consider the prior astrophysical information on the parameters modelling the signal. The prior probability distribution can take on any functional form. Second and more importantly, we want to stress the role played by priors, even when these are non-informative, both in the approximate Fisher analysis and in the standard Bayesian approach. This is done by consistently comparing our prior-informed Fisher results to the full Bayesian results for all of the available GW data from the public Gravitational Wave Transient Catalogs

---

* ulyana.dupletsa@gssi.it

(GWTCs) [2–4].

We structure our work as follows. In Sec. II, we give a brief but comprehensive overview of the analysis technique adopted in our work. In Sec. III, we test our analysis framework against GWTCs data. In Section IV, we provide an overview of our study's findings and highlight the potential and limitations of data-analysis techniques in the GW field. We pay particular attention to the role that assumptions on priors play.

II. ANALYSIS

A. Parameter Estimation

Properties of astrophysical sources from observed GW signals are inferred through Bayesian analysis [22]. This hinges on the Bayes theorem, where the posterior distribution of a given parameter is obtained by combining the prior information, $\pi(\vec{\theta})$, on the parameter with the likelihood, $\mathcal{L}(d|\vec{\theta})$, of observing the given data:

$$p(\vec{\theta}|d) \propto \pi(\vec{\theta})\mathcal{L}(d|\vec{\theta}) \tag{1}$$

The likelihood $\mathcal{L}(d|\vec{\theta})$ is defined as the probability of noise realization:

$$\mathcal{L}(d|\vec{\theta}) \propto \exp\left[-\frac{1}{2}\langle s - h(\vec{\theta})|s - h(\vec{\theta})\rangle\right] \tag{2}$$

where the data s is given by the sum $s = n + h(\vec{\theta}_0)$ of noise n and true signal $h(\vec{\theta}_0)$. $h(\vec{\theta})$ is the theoretical waveform model and depends on the parameters $\vec{\theta}$. Note the difference between the model's parameters $\vec{\theta}$ (the ones we want to infer) and the ones of the actual signal $\vec{\theta}_0$ (unknown).

The inner product $\langle \cdot | \cdot \rangle$ measures the overlap between two signals given the noise characteristics of the detector:

$$\langle a, b \rangle \equiv 4\,\mathrm{Re}\int_{f_{\min}}^{f_{\max}} \frac{\tilde{a}(f)\tilde{b}^*(f)}{S_n(f)} df \tag{3}$$

with $S_n(f)$ the power spectral density of the detector noise. $\tilde{a}(f)$ and $\tilde{b}^*(f)$ are the Fourier transforms of the time-domain signals $a(t)$ and $b(t)$, and $f_{\min}$, $f_{\max}$ the frequency range determined by the sensitivity band of the detector. The noise is assumed to be Gaussian and stationary.

The standard Bayesian analysis estimates the signal parameters, employing Markov Chain Monte Carlo (MCMC) or Nested Sampling algorithms to explore the parameter space and efficiently sample the posterior.

In the Fisher matrix context, the likelihood is assumed to be well approximated by a multidimensional Gaussian. This technique offers a quick and analytic way to estimate the covariance matrix of parameters without offering a straightforward way to take into account prior information.

In the following, we will briefly review the Fisher matrix formalism and then show how to enhance a standard Fisher matrix analysis in post-processing by incorporating physically motivated priors into the posterior samples. To this scope, we will use the GWFish [16] Fisher matrix software and implement a sampling procedure to obtain prior-informed posteriors.

B. Fisher Matrix Formalism

Here we provide a brief introduction to the Fisher matrix method, and refer to [14] for a more detailed analysis.

The Fisher matrix is defined as:

$$F_{ij} = \left\langle \frac{\partial h}{\partial \theta_i}, \frac{\partial h}{\partial \theta_j} \right\rangle\Bigg|_{\theta_{\mathrm{inj}}}, \tag{4}$$

where h is the signal model, $\vec{\theta}_{\mathrm{inj}}$ are the injected parameters used to model the waveform signal $h(\vec{\theta}_{\mathrm{inj}})$, and the inner product is defined in Eq. (3). In Fisher matrix analysis context the injected parameters $\vec{\theta}_{\mathrm{inj}}$ are the true parameters.

The inverse of the Fisher matrix represents the covariance matrix Σ_{ij} of the parameters:

$$\Sigma_{ij} = \left[F^{-1}\right]_{ij} \tag{5}$$

The covariance matrix estimates the uncertainties and correlations in the parameter estimates. The square root of the diagonal elements of Σ_{ij} provides the 1σ uncertainties on the parameters, whereas the off-diagonal terms describe how different parameters are correlated.

C. Integrating Priors into Fisher Matrix Analysis

The Fisher matrix analysis does not include information about the parameters' physical range, not to mention more complicated prior distributions. In the following, we outline the procedure to get prior-informed posteriors, starting from the Fisher matrix. In a few words, this consists of sampling likelihood samples and weighting them by their prior probability.

- The Fisher matrix directly provides the Gaussian likelihood function:

$$\mathcal{L} \propto \exp\left[-\frac{1}{2}\left(\vec{\theta} - \vec{\theta}_{\mathrm{inj}}\right)^{\mathrm{T}} F \left(\vec{\theta} - \vec{\theta}_{\mathrm{inj}}\right)\right] \tag{6}$$

  where F is the Fisher matrix calculated with GWFish and $\vec{\theta}_{\mathrm{inj}}$ are the injected (true) parameters.

- Some parameters (especially angles and spins), even with high SNR, may still be poorly measured and show a largely-spread likelihood. Consequently, when sampling likelihood samples, most

samples lie outside the physical range of parameters. Therefore, we sample directly from the truncated form of the Gaussian likelihood to prevent drawing a large number of samples with null prior, which would have to be discarded. In particular, we rely on the algorithm developed in [23]. This effectively accounts for the parameters' boundaries, ensuring the samples are physically possible.

- For each sample realization drawn from the likelihood, we evaluate the prior probability (see [24] and Appendix B for a more detailed discussion).

- In the final phase of the analysis, we construct the posterior distribution. We start by evaluating the prior probability of each likelihood realization. Then, we choose samples with a weight given by their prior distribution. We normalize the prior probability to ensure it sums up to one across all samples. We use Python's `random.choice` [25] function to select the prior re-weighted samples. The re-weighting process favours samples with higher prior probabilities.

The outlined approach combines the information from the Fisher analysis (via the likelihood) with the additional information provided by the priors. In Fig. 1, we show an example event, the first ever detected GW event, `GW150914`. We plot for each of the 15 parameters 3 sample sets: in *black* the posterior samples provided by LVK, in *red* the median value of the LVK distribution, which we use as the injection for `GWFish`. We superimpose in *orange* the samples obtained from the Fisher analysis alone (likelihood samples) and, in *blue*, the samples we get after the inclusion of priors. It is worth noting how including the prior information for some parameters, especially spins and angles, may play a crucial role and restrict the uncertainty estimates by a large amount. For the parameter descriptions, refer to Tab. IV.

III. COMPARISON WITH GWTC DATA

We conducted an extensive comparison with real data to validate the need to include priors in standard Fisher analysis. To this scope, we recreated the same conditions used for the LVK data analysis and produced our Fisher matrix results.

A. O1 + O2 + O3a+ O3b

We used the updated version (*v2*) of the LVK publicly available GW event database available on `Zenodo` [26] [1] including all the binary black hole (BBH) mergers from

---

[1] GWTC-2.1 for O1 + O2 + O3a and GWTC-3 for O3b

the first 3 observing runs [27, 28]. Specifically, we used the cosmologically reweighted posterior samples labelled as *mixed_cosmo*. In Tab. I we report the comparison of the numbers between all the observed events and those we used in our analysis. In total, we have analyzed 78 events. For a comprehensive list of all the publicly available GW detections and why some of them were not included in our analysis, see Tab. III.

TABLE I. List of detected events during the first 3 observing runs by the LVK Collaboration, compared to those used in our analysis (see Tab. III in Appendix A for further details).

	O1	O2	O3a	O3b	total
observed	3	7	44	36	90
included in our analysis	3	6	36	33	78

B. Fisher analysis

We analysed a total of 78 GW events (see Tab. I and Tab. III). The Fisher analysis of each event was carried out under the same conditions the full Bayesian analysis was obtained. This means:

- Each event has its own detector network with specific sensitivity curves at the moment of detection.

- The waveform approximant is the same and is given by `IMRPhenomXPHM` [29]. This is one of the waveform approximants used in the LVK collaboration for BBH events, readily provided by `LALSimulation` [30].

- The injected values are taken to be the medians of the posterior distributions from the LVK analysis. All the 15 parameters are included in the Fisher analysis: [$\mathcal{M}_c$, q, d_L, θ_{JN}, DEC, RA, ϕ, Ψ, t_c, a_1, a_2, tilt$_1$, tilt$_2$, phi$_{12}$, phi$_{jl}$]. See Tab. IV for a detailed description.

All of this information is publicly available on `Zenodo`.

C. Full posterior reconstruction

Starting from the Fisher results, we follow the method outlined in Sec. II to obtain the posterior samples. The Fisher posterior samples, with and without the addition of priors, are then compared to the ones obtained with the full Bayesian analysis. Therefore, we have adopted the same priors as the full Bayesian procedure to ensure consistent comparison. The specific priors are reported in Tab. II.

We show our main results in Fig. 2 and in Fig. 3. In Fig. 2, for each of the 15 parameters, we plot the ratio between the 90% credible interval we get from the Fisher analysis, without (in *orange*) and with priors (in *blue*),
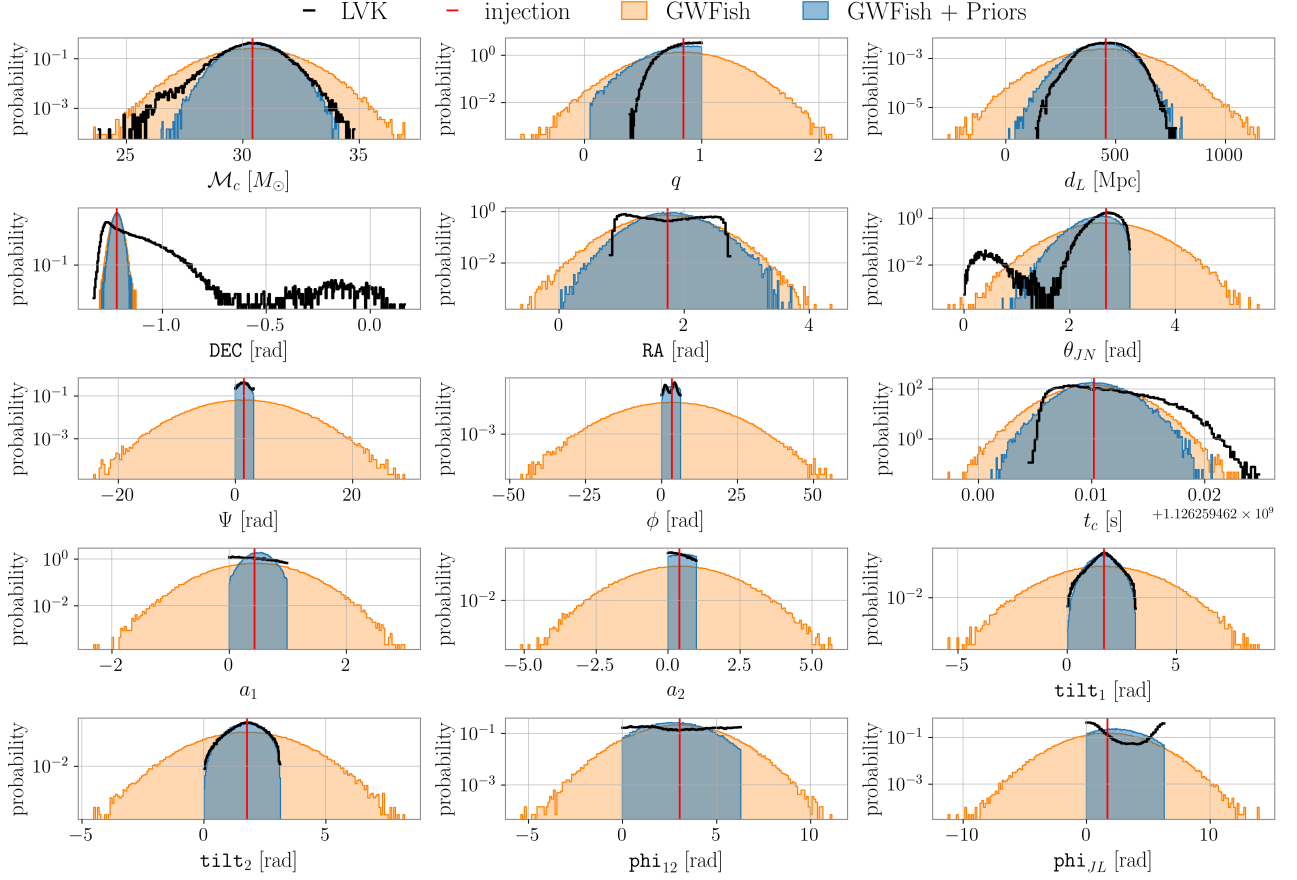
FIG. 1. Comparison of posterior samples probability distribution for all the 15 parameters for the first event `GW150914`. In *black*, we show the LVK samples. Then, in *orange* and *blue* respectively, are the posterior samples obtained using Fisher matrix analysis alone and with priors. The vertical *red* line is the median of the LVK posterior distribution and the injection in our Fisher analysis.

and the 90% credible interval that was obtained with the full Bayesian approach, as a function of the total mass of the binary (in detector frame). Furthermore, the size of the dots is proportional to the SNR of the signal (ranging in $[\sim 2, \sim 24]$), and the colour shade indicates whether the event was seen by 2 (lighter shade) or 3 detectors (darker shade). The SNR obtained in each of the detectors and for the network are listed in detail in Tab. III. Fig. 3 shows the corresponding histograms of the 90% credible interval ratio for each parameter, with (in *blue*) and without (in *orange*) priors. This provides a clearer view of the range of errors and the effect of adding priors. Here are the observations:

- *mass parameters*: The Fisher analysis tends to overestimate chirp mass and mass ratio errors. The match with LVK results is better for the chirp mass. When priors are included, the match becomes very good, and most of the bias of the error estimates (towards larger or smaller errors) is removed.

- *luminosity distance*: The Fisher analysis typically overestimates errors of the luminosity distance, es-

pecially when the number of detectors is lower (2 instead of 3). The inclusion of priors leads to a good match with LVK results. When all three detectors are active, the constraint on the distance measurement is already done well by the Fisher analysis alone.

- *angular parameters*: The inclusion of priors does not generally improve the error estimates of `RA`, `DEC`, and the difference between LVK results and Fisher analysis spans over two orders of magnitude. θ_{JN}, Ψ and ϕ show a slight improvement from priors. We address this specifically in a distinct Sec. III C 1 below.

- *time of coalescence*: The error on t_c is already well estimated with Fisher analysis alone. It is curious to observe that when priors are included in the `GWFish` analysis, the errors of the merger-time estimates can be significantly underestimated.

- *spin parameters*: All the spin parameters are poorly constrained with Fisher analysis alone. In-

TABLE II. List of analytic priors for each parameter entering the description of a GW event. For a more detailed description of the parameters refer to Tab IV.

parameter	units	prior	prior range
$\mathcal{M}_c$	$M_\odot$	Uniform	$[\text{min},\text{max}]$[a]
q	$M_\odot$	Uniform	$[0.05, 1.0]$
d_L	[Mpc]	Power Law, d_L^2	$[10, 10000]$
θ_{JN}	[rad]	Sine	$[0, \pi]$
DEC	[rad]	Cosine	$[-\frac{\pi}{2}, +\frac{\pi}{2}]$
RA	[rad]	Uniform	$[0, 2\pi]$[b]
ϕ	[rad]	Uniform	$[0, 2\pi]$[b]
Ψ	[rad]	Uniform	$[0, \pi]$[b]
t_c	[s]	Uniform	$[t_c - 0.1, t_c + 0.1]$[c]
a_1	-	Uniform	$[0, 0.99]$
a_2	-	Uniform	$[0, 0.99]$
tilt$_1$	[rad]	Sine	$[0, \pi]$
tilt$_2$	[rad]	Sine	$[0, \pi]$
phi$_{12}$	[rad]	Uniform	$[0, 2\pi]$[b]
phi$_{JL}$	[rad]	Uniform	$[0, 2\pi]$[b]

[a] Each event has a specific prior range based on preliminary analysis. The prior interval can be more or less constrained in a case-dependent fashion.
[b] The prior on these parameters has periodic boundary conditions, which cannot be implemented in the context of Fisher analysis.
[c] The prior is roughly plus and minus 0.1 second around the estimated time of arrival, which is the injected value in case of Fisher matrix analysis. In the analysis, though, we have taken exactly the same range as the LVK analysis. This range is reported in the LVK database.

cluding priors allows us to reproduce the LVK results. Still, it should be noted that even the LVK results are likely prior driven since the signals reported in GWTC carried very little information about spins (with some exceptions).

1. Angular Parameters and Multi-Modality

A full Bayesian analysis might encounter multimodality issues, which are not easy to deal with and require some complex and ad-hoc reparametrizations [31]. This happens especially when it comes to angular parameters (see, for example, the theta_JN parameter in Fig. 1). Moreover, it is more evident when fewer detectors are involved, and the SNR in each detector is low (below 4-5). Multi-modality cannot, by definition, be a feature coming out of Fisher's analysis, as it provides a Gaussian likelihood centred around the injected value. This explains the ample range (up to two orders of magnitude) of the ratio between the 90% credible interval obtained with GWFish analysis and the LVK results from full Bayesian analysis as shown in both Fig. 2 and Fig. 3. Generally, the Fisher approximation tends to overestimate the uncertainties, as seen from parameters like the chirp mass, the mass ratio or the luminosity distance. However, when a parameter presents

a multi-modal distribution in standard Bayesian analysis, the Fisher analysis provides poor error estimates as it represents a single mode. Therefore, the constraints from the Fisher analysis are likely to be tighter. To this scope, we selected a subsample of events, for which all 3 detectors were used and the SNR in the Virgo detector was around 4 or higher. As for the two LIGO detectors we did not put any lower threshold for the SNR. This left us with 7 events, GW170814, GW170818, GW190701, GW200202, GW200208, GW200224 and GW200311. The results are shown in Fig. 4. They confirm the general trend discussed before: Fisher analysis alone gives broader or comparable estimates when multi-modality is broken by having more detectors in the analysis.

When it comes to sky localization with ET, multimodality can also be suppressed by observing signals for long periods of time. For example, neutron-star binaries would be observed for hours up to a full day, and this would allow the use of the amplitude and phase modulations of the signal due to the rotation of the Earth to infer the source location.

IV. DISCUSSION AND CONCLUSIONS

In this work, we conducted a thorough analysis of the GWTC data to investigate the effectiveness of Fishermatrix methods and the impact of priors. Our approach involved comparing the posterior samples generated by the LVK collaboration's official Bayesian analysis with the results obtained from our Fisher-matrix software, GWFish. We not only used Fisher analyses alone, but also incorporated a method to apply priors, thus ensuring that our posterior samples were comparable to those generated by the LVK collaboration on an equal basis.

We find that Fisher methods tend to overestimate parameter errors, confirming the findings of [21] (see Fig. 2 and Fig. 3). Adding priors improves the error estimate of parameters like chirp mass, mass ratio, and luminosity distance, especially when few detectors are involved. Priors' impact is even more evident for spin parameters that are poorly constrained by Fisher analyses alone. This is also reflected in the full Bayesian analysis. On the other hand, when it comes to sky location, including priors might only slightly improve the error estimates due to the inherent limitations of the Fisher analysis in handling multi-modal distributions.

Fisher-matrix analyses are always introduced as an approximation valid in the high-SNR limit [14, 21]. The results of this work suggest, instead, that the accuracy of the Fisher analysis is mostly limited by model degeneracies instead of the SNR. The Fisher analysis does well, with a trend to overestimate uncertainties, as long as the parameters are not degenerate and the Bayesian analysis does not output multi-modal posterior distributions. By construction, the Fisher analysis cannot represent multi-modal distributions. Therefore, when multi-modality comes into play, the Fisher analysis represents
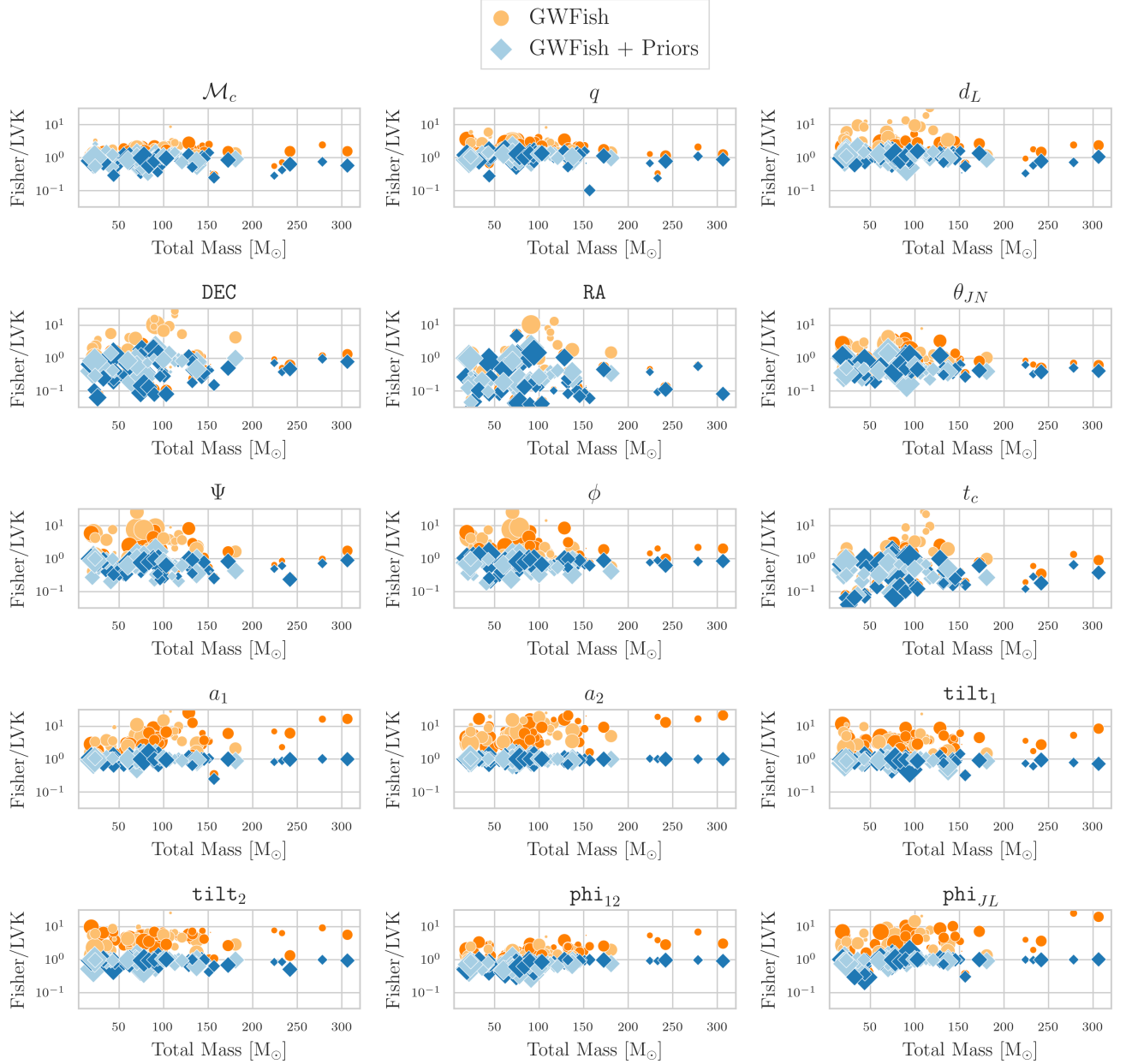
FIG. 2. Plot of the ratio between the 90% credible interval obtained with `GWFish` analysis and the LVK results from full Bayesian analysis. In *orange*, we have the results obtained with `GWFish` only, whereas in *blue*, we added priors in post-processing. Furthermore, the size of the markers reflects the SNR of the signals, which ranges in the interval $[\sim 2, \sim 24]$. The light shade of *orange/blue* signifies that two detectors have made the detection, whereas the darker shade indicates that all three detectors have seen the event.

one of the modes (the one centred around the true parameter value), and this, coming back to angular parameters, explains why the uncertainties on the angular parameters are sometimes better estimated with Fisher approximation than with Bayesian analysis. As we have shown in Fig. 4, degeneracies are broken effectively by having a network of 3 detectors, which not only improves the

match between LVK and `GWFish+Priors` results with respect to sky localization, but in fact improves the match with respect to all parameters. Without priors, the mismatch can still be significant. This highlights the role of priors in taming degeneracies, and it indicates how well `Fisher+Priors` methods work in the absence of important multi-modality in the posterior distribution. Con-
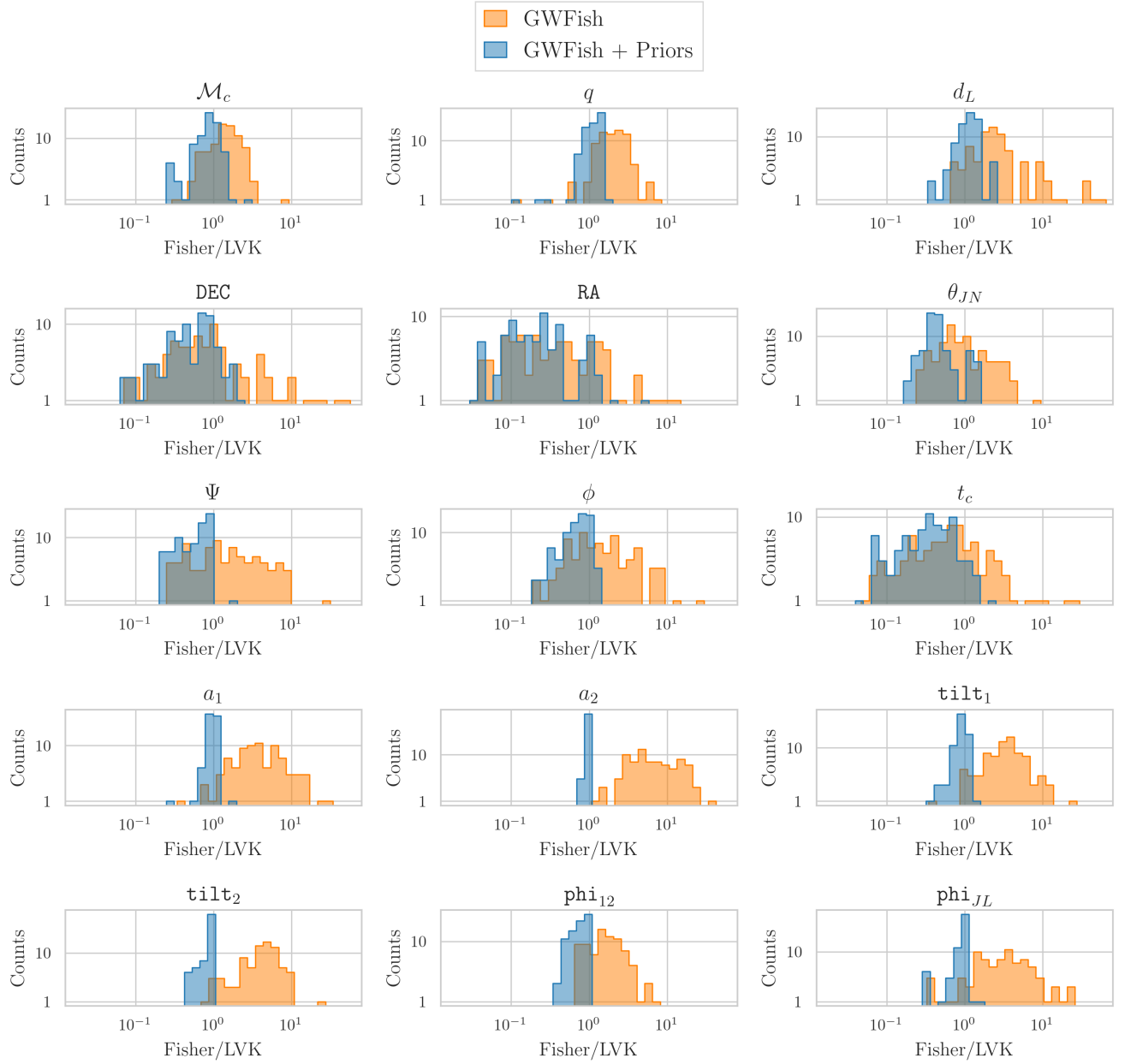
FIG. 3. Histograms of the ratio between the 90% credible interval obtained with `GWFish` analysis and the LVK results from full Bayesian analysis. In *orange*, we have the results obtained with `GWFish` only, whereas in *blue*, we added priors in post-processing.

sequently, the impact of priors in GW data analysis is worth careful consideration.

We conclude that a Gaussian-likelihood approximation is a valid tool to provide estimates of parameter errors, but one needs to understand the limitations of the method. More of the 3-detector observations should be analyzed to corroborate the findings. Still, the results strongly suggest that Fisher-matrix methods, together with priors, provide error estimates that closely match

full Bayesian analyses as long as multi-modality in the posterior distribution of sky locations is absent. Instead, when the sky-localization suffers from multi-modality, the match between LVK results and `GWFish+Priors` is generally worse. Especially the sky-location errors produced by `GWFish+Priors` cannot be trusted in this case. In contrast, error estimates of mass parameters and distance match the LVK results very well, even when the observation is made with only two detectors of the LVK
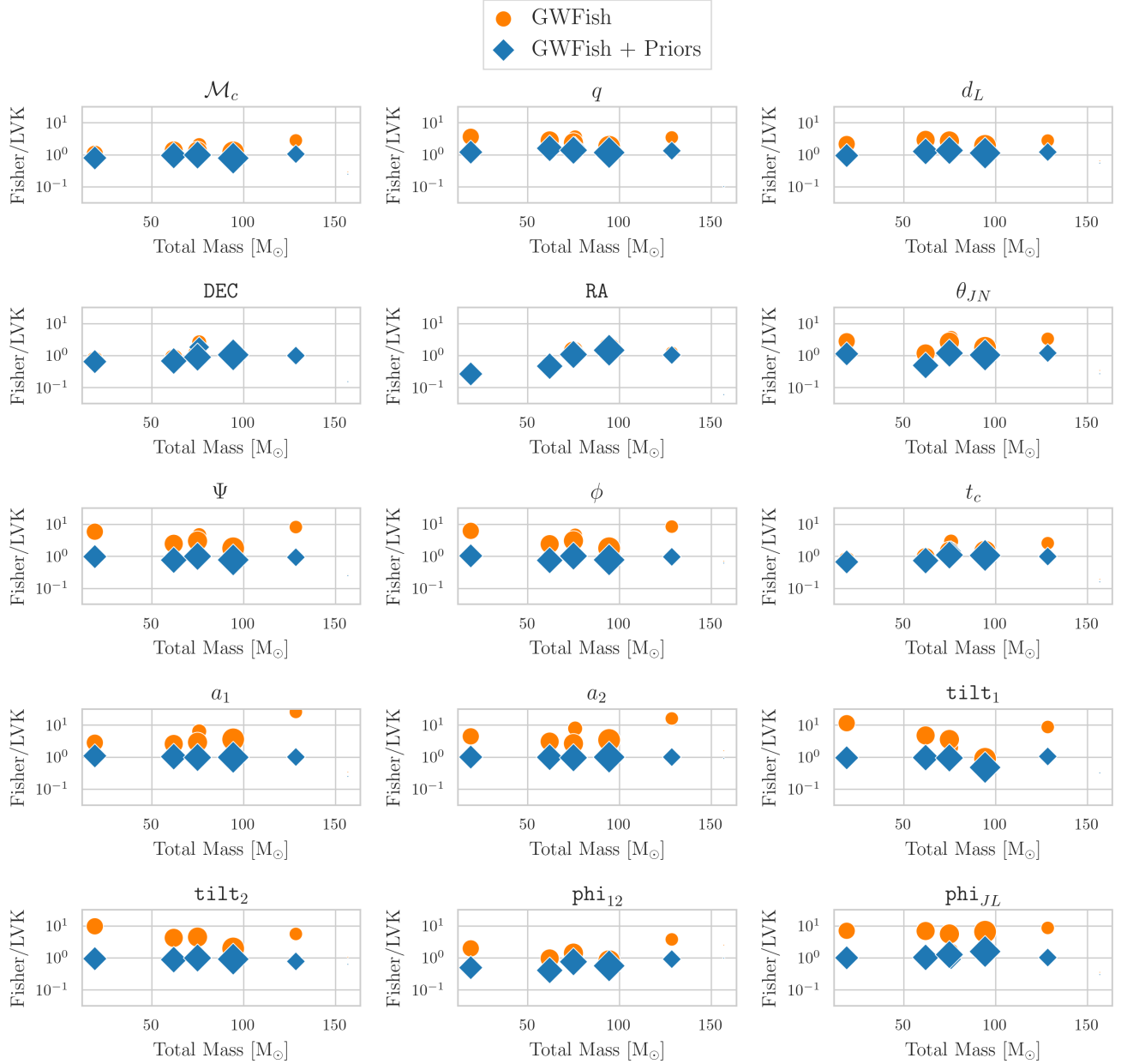
FIG. 4. Same plot as in Fig. 2. Here, the shade of *orange/blue* is the darker one, as in this specific case, we have considered events where all three interferometers were detecting. In particular, we focused on just those events, where the SNR of the signal in the Virgo detector was around ~ 4 or higher (we did not constrain the SNR for the two LIGO detectors).

network.

We want to stress the advantages of using the Fisher+Priors method, particularly for mass and distance estimates, which proved to be the most reliable parameters. The applications can be many, from exploiting tighter constraints when classifying different populations sourcing gravitational-wave signals using machine learning approach [32] to cosmology. Regarding the lat-

ter, gravitational waves are standard sirens as they give direct information on luminosity distance to the source. Therefore, having a reliable and not overestimated distance error makes it possible to put tighter constraints on cosmological parameters, whatever the method used for redshift measurements, either bright or dark sirens [33]. However, one has to pay particular caution to the bright sirens case, as face-on systems may be affected by

degeneracies (distance-inclination angle) that could not be easily resolved, even with priors.

This work corroborates the results obtained in all the science case studies carried out so far with Fisher matrix methods [13, 17, 34–37], with the exception of a few analyses that concern BBH localization with less than three detectors

ACKNOWLEDGMENTS

Appendix A: List of GWTC events

In Table III below, we have listed all the events that were observed during the first three observing runs, excluding the BNS event GW170817 (see Tab. I for a summary). We have highlighted the events that were used in our analysis while also specifying why some events were excluded. Our focus was on BBH sources analyzed with the waveform approximant IMRPhenomXPHM. Events that were not BBH or lacked data about analytical priors were excluded from the study.

TABLE III: List of all observed events during the first 3 observing runs by the LVK Collaboration. The runs have been split into 4 parts, highlighted by different shades of blue, and indicating respectively the data-taking subdivision: O1 (3 events), O2 (7 events plus GW170817), O3-a (44 events) and O3-b (36 events). For each eventID we show if the event is a BBH and, in this case, if it has the analysis with the IMRPhenomXPHM waveform approximant. Furthermore, we signal if the official data report the analytic priors used for the analysis. Finally, we show what detectors have seen the event with the SNR of single detectors and of the network (calculated with GWFish). The last column signals if the event is included in our analysis (in case not the reason why is specified under the column problem).

eventID	BBH	IMRPhenomXPHM	priors	network	GWFish SNR detectors $\rightarrow$ network	problem	included
GW150914_095045	✓	✓	✓	[H1, L1]	$[19.2, 14.3 \rightarrow 23.9]$	-	✓
GW151012_095443	✓	✓	✓	[H1, L1]	$[1.6, 1.6 \rightarrow 2.3]$	-	✓
GW151226_033853	✓	✓	✓	[H1, L1]	$[7.1, 4.6 \rightarrow 8.5]$	-	✓
GW170104_101158	✓	✓	✓	[H1, L1]	$[7.4, 7.2 \rightarrow 10.3]$	-	✓
GW170608_020116	✓	✓	✗	[H1, L1]	-	no priors	✗
GW170729_185629	✓	✓	✓	[H1, L1]	$[3.5, 5.1 \rightarrow 6.2]$	-	✓
GW170809_082821	✓	✓	✓	[H1, L1]	$[1.3, 10.3 \rightarrow 10.4]$	-	✓
GW170814_103043	✓	✓	✓	[H1, L1, V1]	$[3.2, 12.8, 4.0 \rightarrow 13.8]$	-	✓
GW170818_022509	✓	✓	✓	[H1, L1, V1]	$[2.9, 9.2, 3.8 \rightarrow 10.4]$	-	✓
GW170823_131358	✓	✓	✓	[H1, L1]	$[3.5, 3.4 \rightarrow 4.9]$	-	✓
GW190403_051519	✓	✓	✓	[H1, L1, V1]	$[1.3, 3.0, < 1 \rightarrow 3.3]$	-	✓
GW190408_181802	✓	✓	✓	[H1, L1, V1]	$[5.7, 3.5, < 1 \rightarrow 6.8]$	-	✓
GW190412_053044	✓	✓	✓	[H1, L1, V1]	$[9.6, 13.9, 2.9 \rightarrow 17.2]$	-	✓
GW190413_052954	✓	✓	✓	[H1, L1, V1]	$[3.2, 5.6, 2.2 \rightarrow 6.8]$	-	✓
GW190413_134308	✓	✓	✓	[H1, L1, V1]	$[2.2, 5.5, < 1 \rightarrow 6.0]$	-	✓
GW190421_213856	✓	✓	✓	[H1, L1]	$[5.7, 4.1 \rightarrow 7.0]$	-	✓
GW190425_081805	✗	-	-	-	-	no BBH	✗
GW190426_190642	✓	✓	✓	[H1, L1, V1]	$[2.1, 6.1, < 1 \rightarrow 6.5]$	-	✓
GW190503_185404	✓	✓	✓	[H1, L1, V1]	$[5.9, 7.4, 2.5 \rightarrow 9.8]$	-	✓
GW190512_180714	✓	✓	✓	[H1, L1, V1]	$[2.3, 6.7, < 1 \rightarrow 7.2]$	-	✓
GW190513_205428	✓	✓	✓	[H1, L1, V1]	$[7.1, 6.8, 1.6 \rightarrow 10.0]$	-	✓
GW190514_065416	✓	✓	✓	[H1, L1]	$[3.5, 1.2 \rightarrow 3.7]$	-	✓
GW190517_055101	✓	✓	✓	[H1, L1, V1]	$[3.1, 6.6, 3.2 \rightarrow 8.0]$	-	✓
GW190519_153544	✓	✓	✓	[H1, L1, V1]	$[2.7, 3.1, 1.2 \rightarrow 4.3]$	-	✓
GW190521_030229	✓	✓	✓	[H1, L1, V1]	$[2.7, 6.5, < 1 \rightarrow 7.1]$	-	✓
GW190521_074359	✓	✓	✓	[H1, L1]	$[2.9, 17.6 \rightarrow 17.9]$	-	✓
GW190527_092055	✓	✓	✓	[H1, L1]	$[1.2, 4.2 \rightarrow 4.4]$	-	✓
GW190602_175927	✓	✓	✓	[H1, L1, V1]	$[1.9, 6.9, 1.8 \rightarrow 7.4]$	-	✓
GW190620_030421	✓	✓	✓	[L1, V1]	$[10.8, 1.6 \rightarrow 11.0]$	-	✓
GW190630_185205	✓	✓	✓	[L1, V1]	$[10.0, < 1 \rightarrow 10.1]$	-	✓
GW190701_203306	✓	✓	✓	[H1, L1, V1]	$[4.3, 6.8, 4.7 \rightarrow 9.3]$	-	✓

Event				Detectors	Interval		
GW190706_222641	✓	✓	✓	[H1, L1]	$[4.1, 7.6 \to 8.6]$	-	✓
GW190707_093326	✓	✓	✗	[H1, L1]	-	no priors	✗
GW190708_232457	✓	✓	✓	[L1, V1]	$[8.5, < 1 \to 8.5]$	-	✓
GW190719_215514	✓	✓	✓	[H1, L1]	$[2.5, 2.8 \to 3.7]$	-	✓
GW190720_000836	✓	✓	✗	[H1, L1, V1]	-	no priors	✗
GW190725_174728	✓	✓	✗	[H1, L1, V1]	-	no priors	✗
GW190727_060333	✓	✓	✓	[H1, L1, V1]	$[4.4, 6.1, 2.1 \to 7.8]$	-	✓
GW190728_064510	✓	✓	✗	[H1, L1, V1]	-	no priors	✗
GW190731_140936	✓	✓	✓	[H1, L1]	$[1.6, < 1 \to 1.8]$	-	✓
GW190803_022701	✓	✓	✓	[H1, L1, V1]	$[< 1, 4.1, 1.4 \to 4.4]$	-	✓
GW190805_211137	✓	✓	✓	[H1, L1, V1]	$[3.2, 5.0, < 1 \to 6.0]$	-	✓
GW190814_211039	✓	✓	✗	[H1, L1, V1]	-	no priors	✗
GW190828_063405	✓	✓	✓	[H1, L1, V1]	$[8.9, 10.5, 1.4 \to 13.9]$	-	✓
GW190828_065509	✓	✓	✓	[H1, L1, V1]	$[5.0, 3.8, < 1 \to 6.3]$	-	✓
GW190910_112807	✓	✓	✓	[L1, V1]	$[8.8, < 1 \to 8.8]$	-	✓
GW190915_235702	✓	✓	✓	[H1, L1, V1]	$[5.9, 2.3, < 1 \to 6.4]$	-	✓
GW190916_200658	✓	✓	✓	[H1, L1, V1]	$[2.1, 2.2, < 1 \to 3.1]$	-	✓
GW190917_114630	✓	✓	✗	[H1, L1, V1]	-	no priors	✗
GW190924_021846	✓	✓	✗	[H1, L1, V1]	-	no priors	✗
GW190925_232845	✓	✓	✓	[H1, V1]	$[3.1, 4.7 \to 5.7]$	-	✓
GW190926_050336	✓	✓	✓	[H1, L1, V1]	$[2.0, 3.9, < 1 \to 4.4]$	-	✓
GW190929_012149	✓	✓	✓	[H1, L1, V1]	$[1.1, 3.4, < 1 \to 3.5]$	-	✓
GW190930_133541	✓	✓	✓	[H1, L1]	$[2.1, 6.2 \to 6.5]$	-	✓
GW191103_012549	✓	✓	✓	[H1, L1]	$[2.2, < 1 \to 2.3]$	-	✓
GW191105_143521	✓	✓	✓	[H1, L1, V1]	$[2.9, 5.3, 1.2 \to 6.1]$	-	✓
GW191109_010717	✓	✓	✓	[H1, L1]	$[5.0, 9.6 \to 10.8]$	-	✓
GW191113_071753	✓	✓	✓	[H1, L1, V1]	$[3.6, 4.3, < 1 \to 5.6$	-	✓
GW191126_115259	✓	✓	✓	[H1, L1]	$[2.2, 3.6 \to 4.2]$	-	✓
GW191127_050227	✓	✓	✓	[H1, L1, V1]	$[3.6, 2.3, 1.4 \to 4.5]$	-	✓
GW191129_134029	✓	✓	✓	[H1, L1]	$[5.6, 4.4 \to 7.1]$	-	✓
GW191204_110529	✓	✓	✓	[H1, L1, V1]	$[1.9, 5.5 \to 5.8]$	-	✓
GW191204_171526	✓	✓	✓	[H1, L1]	$[9.6, 13.3 \to 16.4]$	-	✓
GW191215_223052	✓	✓	✓	[H1, L1, V1]	$[4.2, 5.7, < 1 \to 7.1]$	-	✓
GW191216_213338	✓	✓	✓	[H1, V1]	$[18.1, 1.8 \to 18.2]$	-	✓
GW191219_163120	✗	-	-	-	-	no BBH	✗
GW191222_033537	✓	✓	✓	[H1, L1]	$[5.2, 1.6 \to 5.5]$	-	✓
GW191230_180458	✓	✓	✓	[H1, L1, V1]	$[5.0, 4.6, 1.2 \to 6.9]$	-	✓
GW200105_162426	✗	-	-	-	-	no BBH	✗
GW200112_155838	✓	✓	✓	[L1, V1]	$[19.3, < 1 \to 19.3]$	-	✓
GW200115_042309	✗	-	-	-	-	no BBH	✗
GW200128_022011	✓	✓	✓	[H1, L1]	$[4.0, 1.8 \to 4.4]$	-	✓
GW200129_065458	✓	✓	✓	[H1, L1, V1]	$[11.7, 19.0, 2.8 \to 22.5]$	-	✓
GW200202_154313	✓	✓	✓	[H1, L1, V1]	$[7.4, 8.7, 3.9 \to 12.1]$	-	✓
GW200208_130117	✓	✓	✓	[H1, L1, V1]	$[2.8, 7.2, 4.7 \to 9.1]$	-	✓
GW200208_222617	✓	✓	✓	[H1, L1, V1]	$[2.9, 4.1, < 1 \to 5.0]$	-	✓
GW200209_085452	✓	✓	✓	[H1, L1, V1]	$[4.2, 2.5, < 1 \to 4.9]$	-	✓
GW200210_092254	✓	✓	✓	[H1, L1, V1]	$[4.7, 6.7, < 1 \to 8.2]$	-	✓
GW200216_220804	✓	✓	✓	[H1, L1, V1]	$[5.7, 3.3, < 1 \to 6.6]$	-	✓
GW200219_094415	✓	✓	✓	[H1, L1, V1]	$[3.3, 4.8, < 1 \to 5.9]$	-	✓
GW200220_061928	✓	✓	✓	[H1, L1, V1]	$[< 1, 3.7, < 1 \to 3.9]$	-	✓
GW200220_124850	✓	✓	✓	[H1, L1]	$[3.0, 1.8 \to 3.5]$	-	✓
GW200224_222234	✓	✓	✓	[H1, L1, V1]	$[11.5, 12.6, 3.9 \to 17.5]$	-	✓
GW200225_060421	✓	✓	✓	[H1, L1]	$[5.5, 5.0 \to 7.4]$	-	✓
GW200302_015811	✓	✓	✓	[H1, V1]	$[2.7, < 1 \to 2.8]$	-	✓
GW200306_093714	✓	✓	✓	[H1, L1, V1]	$[3.2, 1.9, < 1 \to 3.7]$	-	✓
GW200308_173609	✓	✓	✓	[H1, L1, V1]	$[1.1, 2.9, < 1 \to 3.2]$	-	✓
GW200311_115853	✓	✓	✓	[H1, L1, V1]	$[10.1, 9.2, 5.6 \to 14.8]$	-	✓
GW200316_215756	✓	✓	✓	[H1, L1, V1]	$[5.1, 7.2, 2.5 \to 9.2]$	-	✓
GW200322_091133	✓	✓	✓	[H1, L1, V1]	$[1.1, < 1, < 1 \to 1.4]$	-	✓

Appendix B: Prior probability selection in GW Analysis

1. Uniform Prior: the uninformative choice

Most of the parameters characterizing a GW event (see Tab II) have an uninformative uniform prior, meaning that given a physical range of the parameter, any value in the interval is equally probable. The probability density

for a uniform distribution is given by:

$$p(\theta) = \frac{1}{\theta_{\max} - \theta_{\min}} \qquad (B1)$$

where $[\theta_{\min}, \theta_{\max}]$ is the range of the parameter θ. The probability density is zero outside this interval, meaning values out of range are excluded from consideration. Choosing this prior implies that no prior knowledge favours one value over another within the interval.

2. Angular parameters: Uniform on a Sphere prior

While a `Uniform` prior might be the unbiased choice in many contexts, we must consider the spherical geometry when dealing with angular parameters describing positions on a sphere. To ensure a uniform distribution on a sphere, thus isotropy, of certain angular parameters, the right priors are the ones that are uniform in either `Sine` or `Cosine`, depending on the physical range of the angular parameter in consideration.

a. RA and DEC: a detailed analysis

The position in the sky is given by `RA` and `DEC` (see also Fig. 5). The azimuthal angle `RA` ranges in $[0, 2\pi]$ with the zero reference given by the meridian passing through the vernal equinox. The polar angle `DEC` ranges in $[-\pi/2, +\pi/2]$, with zero value at the equator, positive values above and negative below. A uniform distribution on a sphere implies an equal probability of finding an object for any region on the sphere of equal area. This differs from individually considering a uniform distribution for `RA` and `DEC`. The reason is that lines of constant `DEC`, for example, are circles of different sizes, the ones near the pole smaller than the ones near the equator. A uniform prior in `DEC` would lead to a higher concentration of points near the poles.

The correct approach is to consider the area element on the sphere:

$$\begin{aligned} dA &= \sin\left(\frac{\pi}{2} - \text{DEC}\right) d\text{DEC}d\text{RA} \\ &= \cos(\text{DEC})d\text{DEC}d\text{RA} \\ &= d\sin(\text{DEC})d\text{RA} \end{aligned} \qquad (B2)$$

where we have accounted for the fact that `DEC` is not measured starting from the north pole. From Eq. B2, we can see that if `RA` is uniformly distributed in $[0, 2\pi]$, for `DEC` the distribution is uniform in `Sine(DEC)`:

$$p(\sin(\text{DEC})) \propto \text{const} \qquad (B3)$$

where the constant can be found by integrating in the `DEC` range and obtaining const $= 1/2$. We can change variable and directly obtain the prior probability density
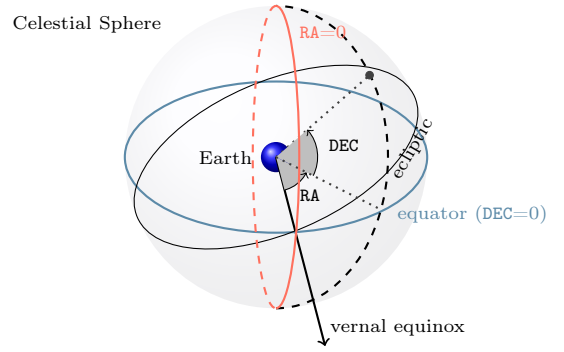

FIG. 5. Schematic representation of angular parameters that describe the position of the source in the sky. `RA` and `DEC` correspond, respectively, to the longitude and latitude on Earth, but in reference to the celestial sphere. The zero reference for `DEC` is the Earth's equator projected onto the celestial sphere. Instead, the zero reference for `RA` is the meridian on the celestial sphere passing through the intersection of the equator line and the ecliptic (vernal equinox). See also Tab. IV.

for declination angle parameter:

$$\begin{aligned} p(\text{DEC}) &= p(\sin(\text{DEC})) \left| \frac{d\sin(\text{DEC})}{d\text{DEC}} \right| \\ &= \frac{1}{2}\cos(\text{DEC}) \quad \text{for} \quad -\frac{\pi}{2} \le \text{DEC} \le +\frac{\pi}{2} \end{aligned} \qquad (B4)$$

b. Angular priors in synthesis

In general, azimuthal angles, like `RA`, follow a uniform distribution in $[0, 2\pi]$. This holds for the phase ϕ, the spin parameters phi_{12} and phi_{jl}, and the polarization angle Ψ. The prior on the polarization angle Ψ, though, is uniform in $[0, \pi]$. The range is not $[0, 2\pi]$ due to the symmetry of the two GW polarizations, h_+ and $h_\times$. In fact, rotating the polarizations by π does not affect the physical configuration of the system, as the polarization angle enters the signal as $\sin(2\Psi)$ or $\cos(2\Psi)$[2]. Taking the range of the polarization angle to be between $[0, \pi]$ allows to avoid redundancy in parameter space, which is particularly useful in Bayesian analysis.

The parameters `theta_JN`, tilt_1 and tilt_2, instead, follow a zenith-like angular distribution as `DEC`. All three are uniformly distributed on the sphere in the range $[0, \pi]$.

---

[2] The dependence on the polarization angle enters the antenna pattern functions:

$$F_+(\theta, \phi, \Psi) = F_{+,0}(\theta, \phi)\cos(2\Psi) - F_{\times,0}(\theta, \phi)\sin(2\Psi)$$
$$F_\times(\theta, \phi, \Psi) = F_{+,0}(\theta, \phi)\sin(2\Psi) + F_{\times,0}(\theta, \phi)\cos(2\Psi)$$

where the $F_{+,0}(\theta, \phi), F_{\times,0}(\theta, \phi)$ are the detector's response to the plus and cross polarizations without considering Ψ. θ and ϕ are related to the sky position of the source (they are functions of `RA` and `DEC`). Do not confuse it with the phase parameter.
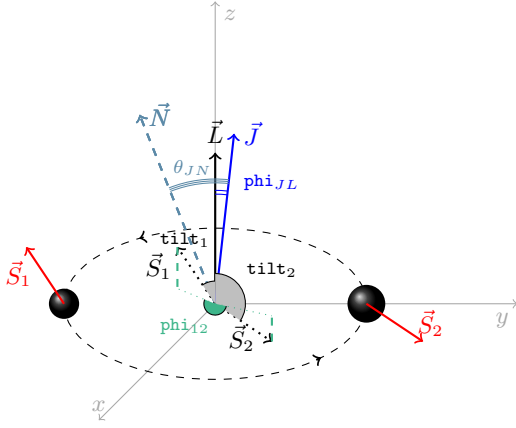
FIG. 6. Schematic view of relevant angular parameters. $\vec{N}$ is the line of sight, connecting the center of Earth to the center of the elliptic orbit. $\vec{L}$ is the orbital angular momentum of the binary, perpendicular to the orbital plane. $\vec{S}_1$ and $\vec{S}_2$ are spin components, with dimensionless magnitude proportional to $a_1 \propto |\vec{S}_1|$ and $a_2 \propto |\vec{S}_2|$. `tilt_1` and `tilt_2` are the angles between $\vec{L}$ and single spin vectors, respectively. `phi_JL` is the angle between $\vec{L}$ and the total momentum $\vec{J}$ (sum of $\vec{L}$, individual spins $\vec{S}_1$, $\vec{S}_2$ and General Relativity corrections). Last, `phi_12` is the angle between the projections of spin vectors on the orbital plane. `theta_JN` is the angle between the line of sight $\vec{N}$ and the total angular momentum $\vec{J}$. `theta_JN` reduces to the inclination angle ι, when the spins of the binary components are aligned to the orbital angular momentum. See also Tab. IV.

This means their Cosine is uniformly distributed. For example, the prior distribution for the `theta_JN` parameter is given by:

$$p(\theta) = \frac{1}{2}\sin(\theta) \quad \text{for} \quad 0 \le \theta \le \pi \tag{B5}$$

which can be obtained in a analogous way as Eq. B4 starting from $p(\cos(\text{DEC})) \propto$ const.

For a comprehensive visualization of the angles refer to Fig. 5 and Fig. 6, and to Tab. IV.

3. Luminosity distance

The prior for the luminosity distance parameter varies according to different assumptions about the distribution of sources in the Universe. In the following, we will explore some common choices.

a. Power Law

In our comparison with LVK data, we used the `Power Law` prior for the luminosity distance, given by:

$$p(d_L) \propto d_L^2 \tag{B6}$$

This choice implies that the number of GW sources is proportional to the volume, assuming a uniform distri-

bution of sources in space without considering any redshift evolution. Since the volume of space scales with the square of the distance ($dV = 4\pi d_L^2 dd_L$), the probability density function is proportional to the square of the source distance. The distance we consider here is the distance we measure, i.e. the luminosity distance.

Choosing this prior assumes that farther events are more likely simply because they cover a larger volume, without accounting for the expansion of the Universe.

b. Uniform in Comoving Volume

If we want to account for the expansion of the Universe, then we should choose the uniform in comoving volume prior:

$$p(d_L) \propto \frac{\mathrm{d}V_c}{\mathrm{d}d_L} = \frac{\mathrm{d}V_c}{\mathrm{d}z}\frac{\mathrm{d}z}{\mathrm{d}d_L} \tag{B7}$$

where we have made explicit the redshift dependence for easier calculations (see also Eq. B11). For the derivative redshift with respect to luminosity distance we compute the inverse, which is easier:

$$\frac{\mathrm{d}d_L}{\mathrm{d}z} = \frac{d_L}{1+z} + \frac{H_0}{c}\frac{1+z}{H(z)} \tag{B8}$$

where

$$d_L = \frac{H_0}{c}(1+z)\int_0^z \frac{\mathrm{d}z'}{H(z')} \tag{B9}$$

and

$$H(z) = \sqrt{(1+z)^3\Omega_{\mathrm{m}} + \Omega_{\Lambda}} \tag{B10}$$

with Ω_{m} and Ω_{Λ} being the dimensionless matter and dark energy densities in the ΛCDM framework.

Eq. B7 takes into account the geometry and the expansion of the Universe. A `Uniform in Comoving Volume` prior favors redshifts where larger volumes are available, in accordance with the cosmological principle of a homogeneous and isotropic Universe.

c. Uniform in Source Frame Time

Furthermore, if we want to assume a constant event rate per unit of time in the source frame, then we have to adjust for the shifting of source frame time:

$$p(d_L) \propto \frac{1}{1+z}\frac{\mathrm{d}V_c}{\mathrm{d}d_L} = \frac{1}{1+z}\frac{\mathrm{d}V_c}{\mathrm{d}z}\frac{\mathrm{d}z}{\mathrm{d}d_L} \tag{B11}$$

The $(1+z)$ factor accounts for the time dilation when passing from source to detector frame:

$$\frac{\mathrm{d}t_{\mathrm{source}}}{\mathrm{d}t_{\mathrm{detector}}} = \frac{1}{1+z} \tag{B12}$$

This prior ensures a uniform event rate in the source frame.

[1] B. Abbott, R. Abbott, T. Abbott, M. Abernathy, F. Acernese, K. Ackley, C. Adams, T. Adams, P. Addesso, R. Adhikari, et al., Physical Review Letters **116** (2016), ISSN 1079-7114, URL http://dx.doi.org/10.1103/PhysRevLett.116.061102.

[2] B. Abbott, R. Abbott, T. Abbott, S. Abraham, F. Acernese, K. Ackley, C. Adams, R. Adhikari, V. Adya, C. Affeldt, et al., Physical Review X **9** (2019), ISSN 2160-3308, URL http://dx.doi.org/10.1103/PhysRevX.9.031040.

[3] R. Abbott, T. Abbott, S. Abraham, F. Acernese, K. Ackley, A. Adams, C. Adams, R. Adhikari, V. Adya, C. Affeldt, et al., Physical Review X **11** (2021), ISSN 2160-3308, URL http://dx.doi.org/10.1103/PhysRevX.11.021053.

[4] R. Abbott, T. Abbott, F. Acernese, K. Ackley, C. Adams, N. Adhikari, R. Adhikari, V. Adya, C. Affeldt, D. Agarwal, et al., Physical Review X **13** (2023), ISSN 2160-3308, URL http://dx.doi.org/10.1103/PhysRevX.13.041039.

[5] S. Hild, S. Chelkowski, and A. Freise, *Pushing towards the et sensitivity using 'conventional' technology* (2008), 0810.0604.

[6] M. Punturo, M. Abernathy, F. Acernese, B. Allen, N. Andersson, K. Arun, F. Barone, B. Barr, M. Barsuglia, M. Beker, et al., Classical and Quantum Gravity **27**, 194002 (2010), URL https://dx.doi.org/10.1088/0264-9381/27/19/194002.

[7] S. Hild, M. Abernathy, F. Acernese, P. Amaro-Seoane, N. Andersson, K. Arun, F. Barone, B. Barr, M. Barsuglia, M. Beker, et al., Classical and Quantum Gravity **28**, 094013 (2011), ISSN 1361-6382, URL http://dx.doi.org/10.1088/0264-9381/28/9/094013.

[8] D. Reitze, R. X. Adhikari, S. Ballmer, B. Barish, L. Barsotti, G. Billingsley, D. A. Brown, Y. Chen, D. Coyne, R. Eisenstein, et al., *Cosmic explorer: The u.s. contribution to gravitational-wave astronomy beyond ligo* (2019), 1907.04833.

[9] M. Evans, R. X. Adhikari, C. Afle, S. W. Ballmer, S. Biscoveanu, S. Borhanian, D. A. Brown, Y. Chen, R. Eisenstein, A. Gruson, et al., *A horizon study for cosmic explorer: Science, observatories, and community* (2021), 2109.09882.

[10] G. Ashton, M. Hübner, P. D. Lasky, C. Talbot, K. Ackley, S. Biscoveanu, Q. Chu, A. Divakarla, P. J. Easter, B. Goncharov, et al., The Astrophysical Journal Supplement Series **241**, 27 (2019), ISSN 1538-4365, URL http://dx.doi.org/10.3847/1538-4365/ab06fc.

[11] I. M. Romero-Shaw, C. Talbot, S. Biscoveanu, V. D'Emilio, G. Ashton, C. P. L. Berry, S. Coughlin, S. Galaudage, C. Hoy, M. Hübner, et al., Monthly Notices of the Royal Astronomical Society **499**, 3295–3319 (2020), ISSN 1365-2966, URL http://dx.doi.org/10.1093/mnras/staa2850.

[12] G. Ashton and C. Talbot, Monthly Notices of the Royal Astronomical Society **507**, 2037–2051 (2021), ISSN 1365-2966, URL http://dx.doi.org/10.1093/mnras/stab2236.

[13] M. Branchesi, M. Maggiore, D. Alonso, C. Badger, B. Banerjee, F. Beirnaert, E. Belgacem, S. Bhagwat, G. Boileau, S. Borhanian, et al., Journal of Cosmology and Astroparticle Physics **2023**, 068 (2023), ISSN 1475-7516, URL http://dx.doi.org/10.1088/1475-7516/2023/07/068.

[14] M. Vallisneri, Phys. Rev. D **77**, 042001 (2008), gr-qc/0703086.

[15] S. Borhanian, Classical and Quantum Gravity **38**, 175014 (2021), ISSN 1361-6382, URL http://dx.doi.org/10.1088/1361-6382/ac1618.

[16] U. Dupletsa, J. Harms, B. Banerjee, M. Branchesi, B. Goncharov, A. Maselli, A. C. S. Oliveira, S. Ronchini, and J. Tissino, Astronomy and Computing **42**, 100671 (2023), 2205.02499.

[17] F. Iacovelli, M. Mancarella, S. Foffa, and M. Maggiore, The Astrophysical Journal **941**, 208 (2022), ISSN 1538-4357, URL http://dx.doi.org/10.3847/1538-4357/ac9cd4.

[18] F. Iacovelli, M. Mancarella, S. Foffa, and M. Maggiore, The Astrophysical Journal Supplement Series **263**, 2 (2022), ISSN 1538-4365, URL http://dx.doi.org/10.3847/1538-4365/ac9129.

[19] Y. Li, I. S. Heng, M. L. Chan, C. Messenger, and X. Fan, Phys. Rev. D **105**, 043010 (2022), URL https://link.aps.org/doi/10.1103/PhysRevD.105.043010.

[20] M. L. Chan, C. Messenger, I. S. Heng, and M. Hendry, Phys. Rev. D **97**, 123014 (2018), URL https://link.aps.org/doi/10.1103/PhysRevD.97.123014.

[21] C. L. Rodriguez, B. Farr, W. M. Farr, and I. Mandel, Physical Review D **88** (2013), ISSN 1550-2368, URL http://dx.doi.org/10.1103/PhysRevD.88.084013.

[22] E. Thrane and C. Talbot, Publications of the Astronomical Society of Australia **36** (2019), ISSN 1448-6083, URL http://dx.doi.org/10.1017/pasa.2019.2.

[23] Z. I. Botev, Journal of the Royal Statistical Society Series B: Statistical Methodology **79**, 125–148 (2016), ISSN 1467-9868, URL http://dx.doi.org/10.1111/rssb.12162.

[24] T. Callister (2021), 2104.09508.

[25] C. R. Harris, K. J. Millman, S. J. van der Walt, R. Gommers, P. Virtanen, D. Cournapeau, E. Wieser, J. Taylor, S. Berg, N. J. Smith, et al., Nature **585**, 357 (2020), URL https://doi.org/10.1038/s41586-020-2649-2.

[26] European Organization For Nuclear Research and OpenAIRE, *Zenodo* (2013), URL https://www.zenodo.org/.

[27] T. L. S. Collaboration, the Virgo Collaboration, R. Abbott, T. D. Abbott, F. Acernese, K. Ackley, C. Adams, N. Adhikari, R. X. Adhikari, V. B. Adya, et al., *Gwtc-2.1: Deep extended catalog of compact binary coalescences observed by ligo and virgo during the first half of the third observing run* (2022), 2108.01045.

[28] R. Abbott, T. Abbott, F. Acernese, K. Ackley, C. Adams, N. Adhikari, R. Adhikari, V. Adya, C. Affeldt, D. Agarwal, et al., Physical Review X **13** (2023), ISSN 2160-3308, URL http://dx.doi.org/10.1103/PhysRevX.13.041039.

[29] G. Pratten, C. García-Quirós, M. Colleoni, A. Ramos-Buades, H. Estellés, M. Mateu-Lucena, R. Jaume, M. Haney, D. Keitel, J. E. Thompson, et al., Physical Review D **103** (2021), ISSN 2470-0029, URL

http://dx.doi.org/10.1103/PhysRevD.103.104056.

[30] S. Husa, S. Khan, M. Hannam, M. Pürrer, F. Ohme, X. J. Forteza, and A. Bohé, Phys. Rev. D **93**, 044006 (2016), URL https://link.aps.org/doi/10.1103/PhysRevD.93.044006.

[31] J. Roulet, S. Olsen, J. Mushkin, T. Islam, T. Venumadhav, B. Zackay, and M. Zaldarriaga, Physical Review D **106** (2022), ISSN 2470-0029, URL http://dx.doi.org/10.1103/PhysRevD.106.123015.

[32] F. Santoliquido, U. Dupletsa, J. Tissino, M. Branchesi, F. Iacovelli, G. Iorio, M. Mapelli, D. Gerosa, J. Harms, and M. Pasquato, *Classifying binary black holes from population iii stars with the einstein telescope: a machine-learning approach* (2024), 2404.10048.

[33] A. Cozzumbo and et al., **In Preparation** (2024).

[34] S. Borhanian and B. S. Sathyaprakash, *Listening to the universe with next generation ground-based gravitational-wave detectors* (2024), 2202.11048.

[35] S. Ronchini, M. Branchesi, G. Oganesyan, B. Banerjee, U. Dupletsa, G. Ghirlanda, J. Harms, M. Mapelli, and F. Santoliquido, Astronomy & Astrophysics **665**, A97 (2022), ISSN 1432-0746, URL http://dx.doi.org/10.1051/0004-6361/202243705.

[36] B. Banerjee, G. Oganesyan, M. Branchesi, U. Dupletsa, F. Aharonian, F. Brighenti, B. Goncharov, J. Harms, M. Mapelli, S. Ronchini, et al., Astronomy & Astrophysics **678**, A126 (2023), ISSN 1432-0746, URL http://dx.doi.org/10.1051/0004-6361/202345850.

[37] E. Loffredo and et al., **In Preparation** (2024).

TABLE IV. List of all the parameters in the parametrization used in our analysis. For a better understanding of some definitions refer to Fig 6 and Fig 5.

parameter	label	description
chirp mass	$\mathcal{M}_c$	combination of detector frame masses: $\mathcal{M}_c = \frac{(m_1 m_2)^{3/5}}{(m_1 + m_2)^{1/5}}$
mass ratio	q	ratio between the secondary and the primary component masses, $0 < q \leq 1$
luminosity distance	d_L	luminosity distance to the source
theta_JN	θ_{JN}	angle between the line of sight $\vec{N}$ the total angular momentum of the binary $\vec{J}$
declination	DEC	coordinate on celestial sphere corresponding to latitude on Earth
right ascension	RA	coordinate on celestial sphere corresponding to longitude on Earth
phase	ϕ	phase of the gravitational wave at the coalescence
polarization angle	Ψ	rotation of GW polarizations reference frame with respect to detector's arms in Earth's frame
geocentric time	t_c	merger time, calculated as GPS time
a_1	a_1	dimensionless spin magnitude of primary component
a_2	a_2	dimensionless spin magnitude of secondary component
tilt_1	$\mathtt{tilt}_1$	angle between the spin vector of primary component and the orbital angular momentum $\vec{L}$
tilt_2	$\mathtt{tilt}_2$	angle between the spin vector of secondary component and the orbital angular momentum $\vec{L}$
phi_12	$\mathtt{phi}_{12}$	angle between the projections of the two spin vectors onto the orbital plane
phi_jl	$\mathtt{phi}_{JL}$	angle between the orbital angular momentum $\vec{L}$ and the total angular momentum $\vec{J}$